JOURNAL OF
HYDRO-METEOROLOGY



*Research Article*

# Development of a prototype system of the very short-range forecast of precipitation in Vietnam

**Kazuo Saito[1,2,3]*, Mai Khanh Hung[4], Du Duc Tien[4]**

[1] Japan Meteorological Business Support Center, Tokyo101-0054, Japan; k-saito@jmbsc.or.jp
[2] Atmosphere and Ocean Research Institute, University of Tokyo, Kashiwa 277-8564, Japan; k_saito@aori.u.tokyo.ac.jp
[3] Meteorological Research Institute, Japan Meteorological Agency, Tsukuba 305-0052, Japan; ksaito@mri-jam.go.jp
[4] National Center for Hydro-Meteorological Forecasting, Hanoi 10000, Vietnam; maikhanhhung18988@gmail.com; duductien@gmail.com

*Corresponding author: k-saito@jmbsc.or.jp; Tel.: +813–55772178

Received: 6 March 2023; Accepted: 14 April 2023; Published: 25 June 2023

**Abstract:** We developed a prototype system of the very short-range forecast of precipitation in Vietnam by merging kinematic extrapolations of composite hourly rainfall analysis and NWP, verified its performance for the case of a heavy rainfall event in July 2021 over central Vietnam. First, we produced hourly composite rainfall analysis over Vietnam with a grid distance of 5 km using AWS, radar, and satellite data. Next, we computed lag correlations between two hourly rainfall intensities at specific templates of 50 × 50 grids, and obtained lag indexes that maximize the lag correlation at 11 × 10 points. The moving vectors of precipitation areas at all grids are obtained by Cressman interpolation of the lag indexes, and a quality check using NWP horizontal winds at 700 hPa level was applied. Kinematic extrapolation of rainfall analysis was conducted using the above moving vectors and was merged with hourly rainfall prediction by a regional NWP model at NCHMF of VNMHA (WRF3kmIFS-DA) by weighted averaging. The magnitude of weight for the NWP in the merger was linearly increased from 0 to 1 for FT = 2 to 6 (from 03 UTC to 07 UTC, 12 July 2021). Verifications showed that the merged rainfalls outperformed both NWP and kinematically extrapolated precipitations for the time range of FT = 3 to 5.

**Keywords:** Precipitation analysis; Radar composite; Quantitative precipitation forecast; Very short-range forecast of precipitation.

## 1. Introduction

In most countries in southeast and east Asia including Vietnam and Japan, meteorological disasters occur every year. In particular, disasters by heavy rains often cause the greatest damage, and improvement of nowcasting and forecasting of intense precipitation is a key issue for disaster prevention and mitigation. Since June 2018, a bilateral cooperation project between the Japan International Cooperation Agency (JICA) and the Viet Nam Meteorological and Hydrological Administration (VNMHA) for "Strengthening Capacity in Weather Forecasting and Flood Early Warning System in the Social Republic of Vietnam" has been conducted. The Japan Meteorological Business Support Center (JMBSC) has been participating in the project as a main contributing organization of Japan. The project scopes are divided into four output targets: 1) surface meteorological observation; 2) radar

maintenance and products; 3) weather forecasting; and 4) regional weather dissemination. More detailed reviews of the JICA project are given by [1].

One of the main targets of the JICA project is quantitative precipitation estimation (QPE). QPE focuses on estimating precipitation levels over a relatively short period, such as a few hours in disaster prevention. QPE is useful in predicting the likelihood of flash floods or other weather–related hazards in a given area. Good QPE is attained by qualified networks of rain gauges and radars, and satellite data are used for supplementary information for filling data sparse areas as on the sea. In the first term of the JICA project, maintenance and installation of automated rain gauges for radar QPE calibration [2], and QPE by combining rain gauge and meteorological radar network [3] in Vietnam were conducted. At the National Center for Hydro-Meteorological Forecasting (NCHMF) of VNMHA, precipitation nowcasting for 3-hour precipitation is operationally conducted using a composite of rain gauge data at Automated Weather Stations (AWS), rainfall estimation by radars and satellite (Himawari-8 or GPS) [4–5].

Another important topic in disaster prevention is the quantitative precipitation forecast (QPF). QPF is typically based on numerical weather prediction (NWP), and short-term QPFs are used for decisions about pre-evacuation and emergency response. Although the accuracy of NWP has improved remarkably in recent years, the absolute accuracy of NWP is still not necessarily sufficient for disaster prevention, especially in a very short range of time (e.g., less than 6 hours), where the accuracy is often inferior to the kinematic extrapolation of the precipitation analysis. To bridge this gap between QPE and NWP, the Japan Meteorological Agency (JMA) operates its precipitation analysis and very short-range forecast of precipitation (VSRFP). The first one is the precipitation nowcast based on radar/rain gauge-analyzed precipitation with a spatial resolution of 250-1000 m, updated every 5 minutes [6].

VSRFP of JMA predicts precipitation with a spatial resolution of 1 km up to 6 hours ahead, updated every 10 minutes, whose basic concept is the merge of kinematic extrapolation of precipitation analysis and regional NWP model forecasts. Since performance of kinematic extrapolation deteriorates more rapidly than NWP, VSRFP with merging usually outperforms both extrapolation and NWP (Figure 1) [7–8].

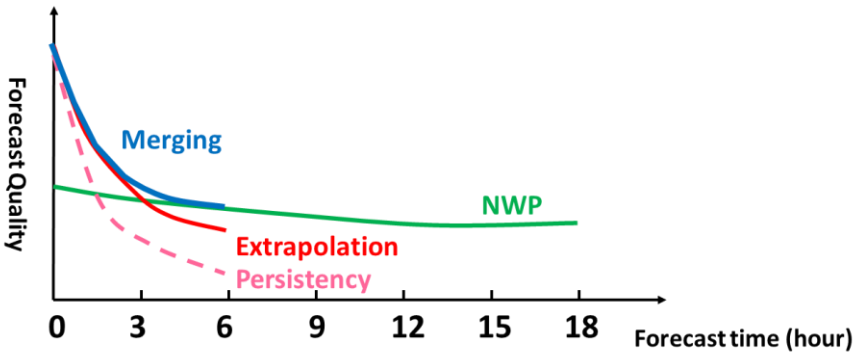


**Figure 1.** Concept of VSRFP: Reproduced from Saito and Makihara (2007) [7].

A similar precipitation nowcasting system, SWIRLS, has been in operation at the Hong Kong Observatory as well [9]. At JMA, both precipitation nowcast and VSRFP are essential information to issue advisories and warnings for rainfall and are used as input data for its hydrological model to compute soil water, surface water, and runoff indexes on risks of landslide, inundation, and river flood [10]. The importance of such the impact-based forecasting (IBF [11]) is increasing in several countries that suffer from natural disasters including Vietnam. Toward the realization of a very short-range rainfall prediction system in Vietnam similar to VSRFP of JMA, we developed a prototype system of the very short-range forecast of precipitation in Vietnam by merging kinematic extrapolations of composite hourly

rainfall analysis and regional NWP at NCHMF. Validation of the system was conducted for a heavy rainfall event that occurred in central Viet Nam in September 2021.

The organization of this paper is as follows. In Section 2, a heavy rainfall event in central Vietnam on 10-12 September 2021 is introduced. In Section 3, hourly composite rainfall analysis for this case using AWS, radar, and satellite data is described. The performance of persistency for this case is shown with verification scores. In Section 4, the kinematic extrapolation method for rainfall areas by moving vectors based on lag correlation is described. Quality control of moving vectors is performed by checking consistency against NWP winds. In section 5, a merge of extrapolated rains with regional NWP at NCHMF is described, with its verification scores. Summary and concluding remarks are given in Section 6.

## 2. Heavy rainfall event in central Viet Nam on 10-12 September 2021

On September 10-12, 2021, a heavy rainfall event occurred in central Vietnam, and at Danang, rain of 584 mm was observed in 48 hours from 12 UTC Sep 10 to Sep 12 (Figure 2). This heavy rainfall was brought by a weak tropical cyclone (T2113 Conson), which moved westward over the East China sea (Figure 3a). Although its intensity was not strong in terms of the central pressure (Figure 3b), this tropical cyclone was accompanied by a distinct cold dense overcast as seen in the Himawari satellite images (Figure 4).

As shown in Figure 2a, there were two peaks in this heavy rainfall event; 1012 UTC to 1112 UTC, and 1118 UTC to 1212 UTC. Here, we focus on the later peak of the rainfall in this study. Figure 5 indicates SYNOP and AWS 6h rains for 1118-1212 UTC. Generally, AWS rainfall well follows the rainfall pattern in SYNOP and indicates a more detailed distribution. Quality control of AWSs in Vietnam has been discussed by [11].

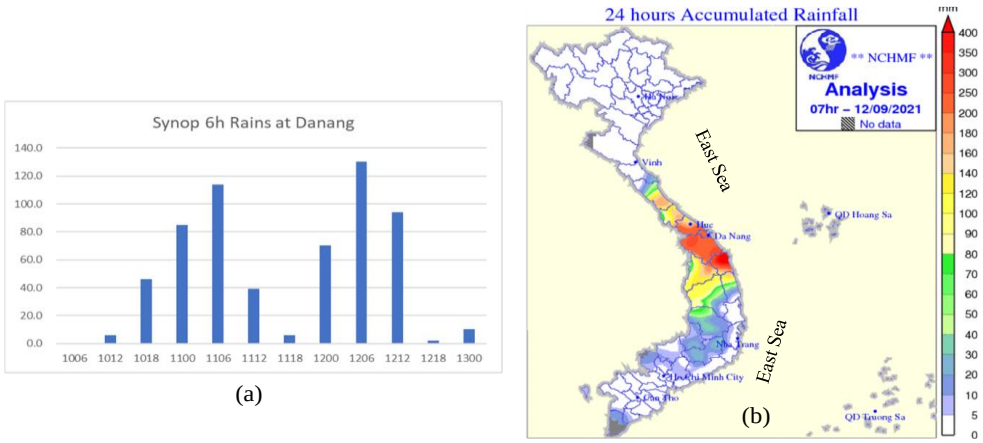


**Figure 2.** (a) SYNOP 6h observed rain at Danang 584 mm in 48h from 12 UTC Sep 10 to 12 UTC Sep 12; (b) SYNOP 24h accumulated rain at 12 UTC Sep 12.

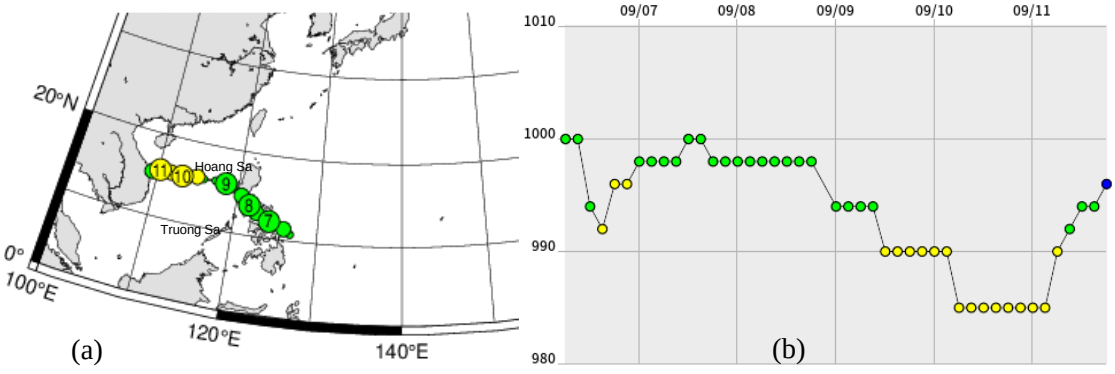


**Figure 3.** Track (a) and central pressure (b) of typhoon T2113 Conson. After the Digital Typhoon website of the National Institute of Informatics (http://agora.ex.nii.ac.jp/digital-typhoon/summary/wnp/s/202113.html.en).

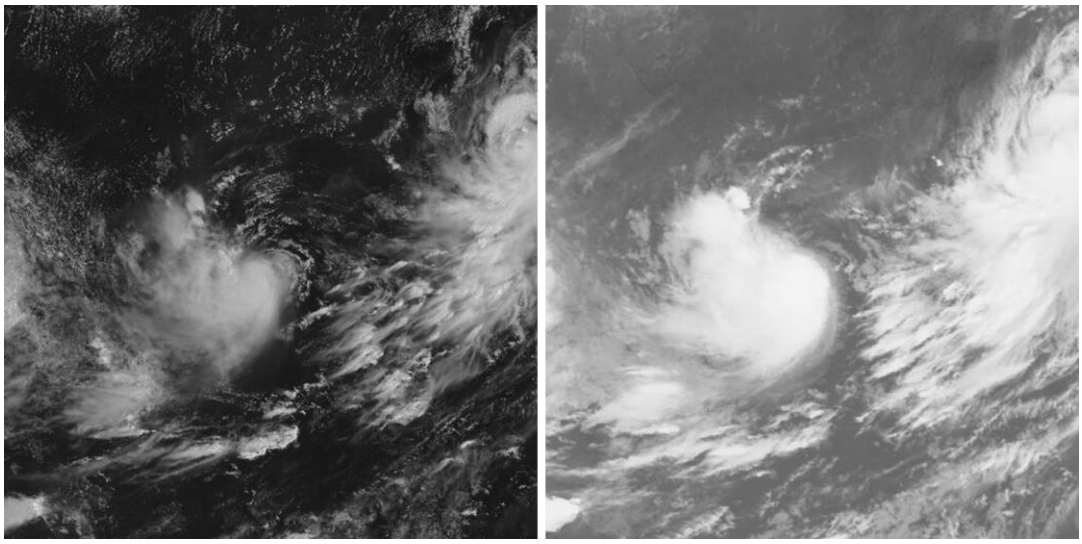

**Figure 4.** Himawari-8 satellite images at 202109 1103UTC for VIS (left) and IR (right).

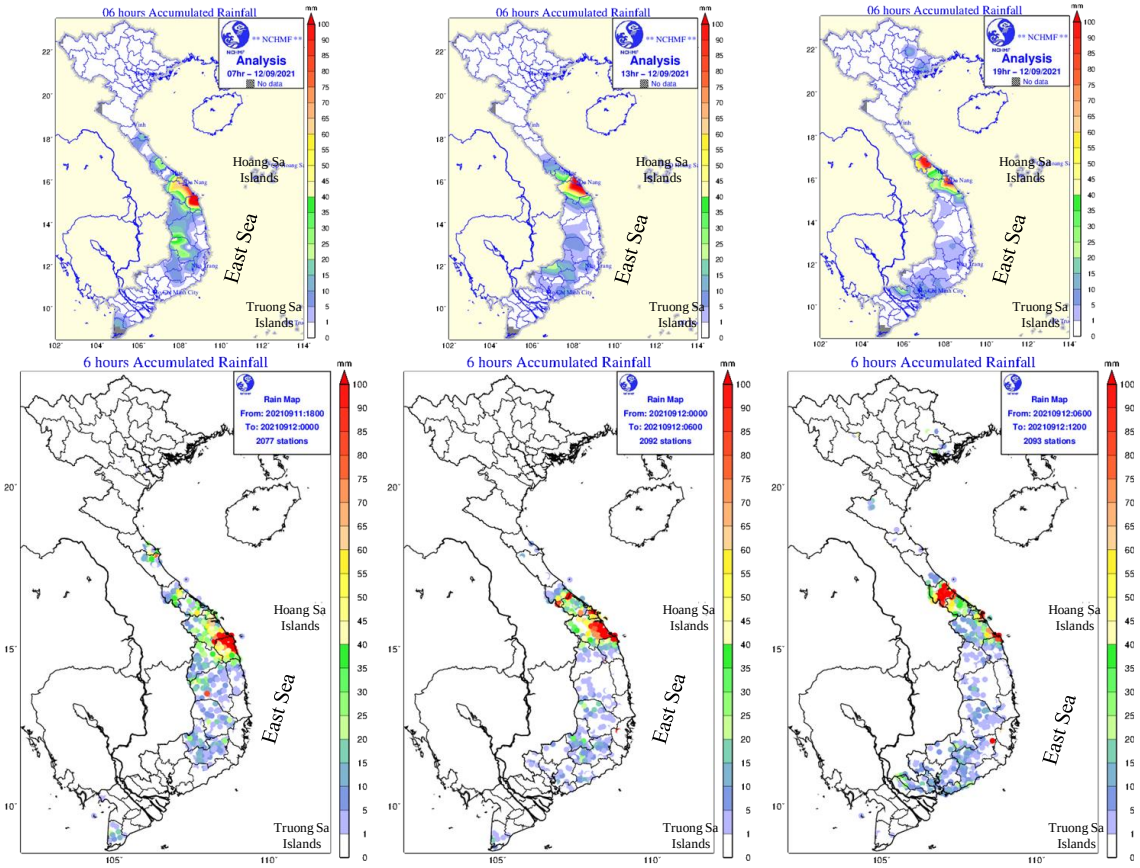


**Figure 5.** Upper) SYNOP 6h rains for 2021 September 11th 18 UTC to 12th 12 UTC. Lower) AWS 6h rains.

## 3. Hourly composite rainfall analysis

### *3.1. Hourly precipitation nowcast*

VNMHA has operationally produced a 3-hour accumulated rainfall analysis using a composite of AWS, radar, and satellite estimated rainfall since August 2018. These observation data are collected by AMO of VNMHA daily, and binary-formatted precipitation amount data are prepared with a horizontal grid spacing of 0.05 degree. For details of meteorological radar observations at VNMHA and rainfall estimate from radars [2]. As

described by [4], two kinds of precipitation analysis ("Mean" and "Max") are produced at NCHMF. In "Mean", a priority order of data, AWS, radar and satellite, is prescribed, and precipitation amount at each analysis grid is determined by higher priority data source in order among the available data (e.g., a mean value of AWS precipitation is taken first if AWS rain gauge data are available). In "Max", the maximum value of the available data is selected.

In this study, to develop a very short-range forecast of precipitation system, first, we modified the rainfall analysis from three hourly to one hour. Figure 6 shows hourly rainfall at 00 UTC (07 LST; upper) and 01 UTC (08 LST; lower) of 2021 Sep 12 by AWS, radar, satellite, and their composite precipitation. Same as in Saito et al (2020), the composite rain map for the domain from 8.5 N to 23.5 N and 102.0 E to 116.0 E with a grid spacing of 0.05 degree is made with a priority in the order of AWS, radar, and satellite (i.e., same as "Mean"). Both the AWS and radar detected intense rains over central Vietnam. In the satellite estimated rainfall, very intense rains over 40 mm/h are seen not only over the central part of Vietnam, but in Thailand and over the South China Sea, corresponding to low TBB areas shown in the IR image in Figure 4. As discussed in [4–5], these very intense rainfalls are likely overestimation by using the statistical relationship between the cloud top temperature and rainfall by [12]:

$$R = 1.1183\times10^{11}\exp(-3.6382\times10^{-2}T_{BB}^{1.2}) \quad (1)$$

This relationship yields extremely intense rains (R) if the satellite-observed cloud top temperature ($T_{BB}$) is very low. This over-estimation by satellite is masked by AWS and radar rainfall in the composited rains over the mainland of Vietnam. Figure 7 indicates hourly composite rainfall analyses for successive 4 hours from 02 to 07 UTC, 2021 Sep 12.

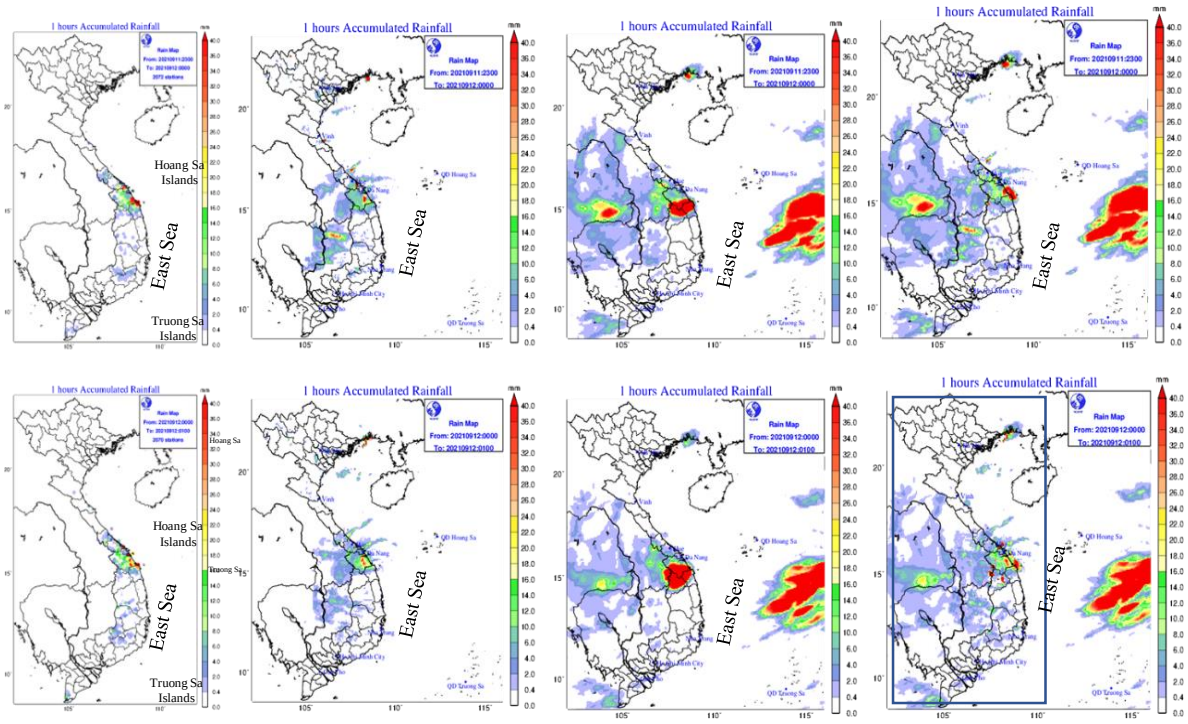


**Figure 6.** Upper) Hourly rainfall at 2021 Sep 12 00UTC (07LST) by AWS, radar, satellite, and composite precipitation. Lower) Same as upper but for 01 UTC (08 LST).

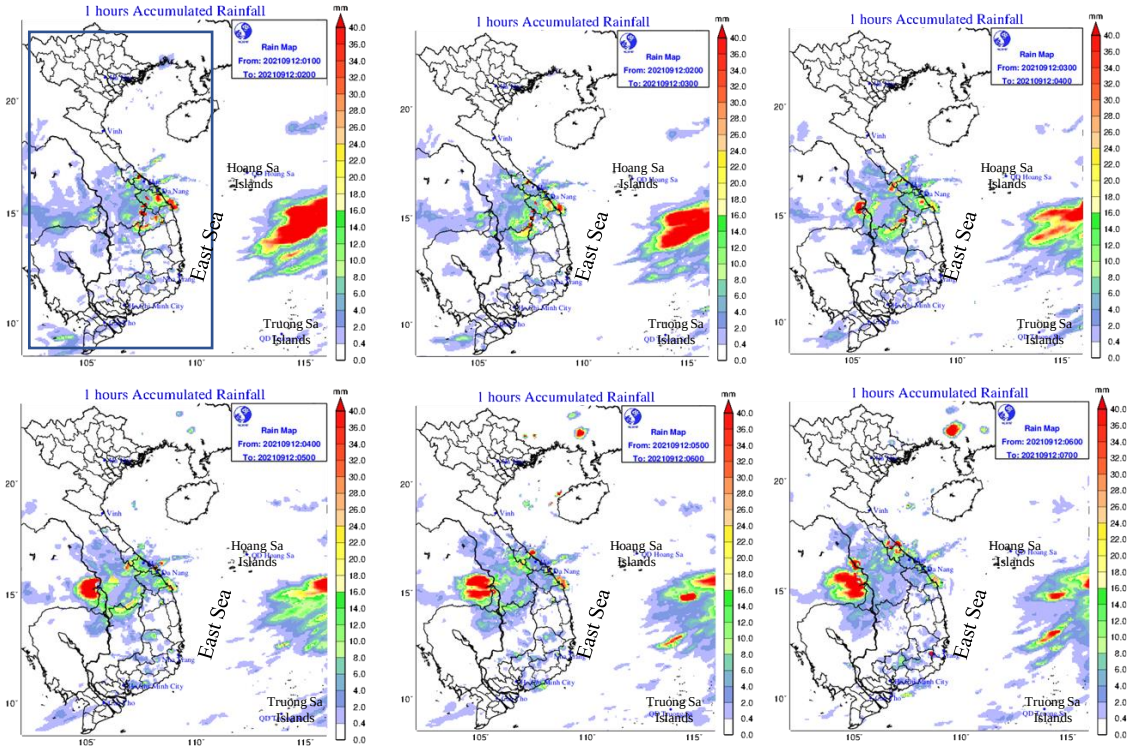


**Figure 7.** Composited hourly precipitation nowcast from 02UTC to 07 UTC, 2021 Sep 12.

### *3.2. Verification of persistency*

Before the discussion on extrapolation of the rainfall areas, first we checked the performance of the persistency of hourly rainfall analysis in this heavy rainfall event. Considering the tendency of overestimation of intense rains in satellite rainfall estimation, the verification area is confined around the mainland of Vietnam, indicated by rectangles shown in Figures 6 and 7.

Figures 8 and 9 show scatter diagrams that indicate correlations of rainfall intensities from 02 UTC to 07 UTC against the rainfall intensity at 01 UTC in the verification domain. Needless to say, if we take the same time (01 UTC), the scatter plots are on the diagonal line of x = y. With the one-hour time lag (02 UTC), the scatter diagrams show a dispersion apart from the diagonal line, and this dispersion gradually increases with time. Middle and lower panels of Figure 8 show bias and threat scores of the persistency respectively, for different intensity thresholds from 0.5 to 20 mm/h, where the composite rains at 01 UTC are regarded as the forecast and the analyses at 02 to 07 UTC are regarded as the observation. At 02 to 03 UTC, bias scores are around 1.0 for all thresholds, while after 04 UTC, bias scores tend to decrease for intense rains. The threat scores tend to decrease with time, especially for intense rains. At 02 UTC, threat scores are about 0.55 at 0.5 mm/h and around 0.25 for rains over 5 mm/h. After 05 UTC, threat scores for intense rains over 10 mm/h become smaller than 0.1, however, in this case, threat scores for weak rains such as 0.5 mm/h keep their values around 0.4 (Figure 9).

Figure 10 shows the time evolution of bias scores (upper panels) and threat scores (lower panels) for weak (1 mm/h) and moderate (5 mm/h) rains from 01 to 07 UTC (FT = 0 to 6). In these rainfall intensity ranges, bias scores keep their values around unity for the whole verification period. Threat scores rapidly decrease at the first one to two hours but remain at a certain value even after FT = 3. Usually, in the middle latitude region such as in Japan, rainfall areas are advected eastward by the westerly, thus the threat scores persistency become very small with time. In this case study, the major rainfall areas by tropical cyclone remained over Vietnam, thus both bias and threat scores of the persistency kept its performance even after FT = 3.

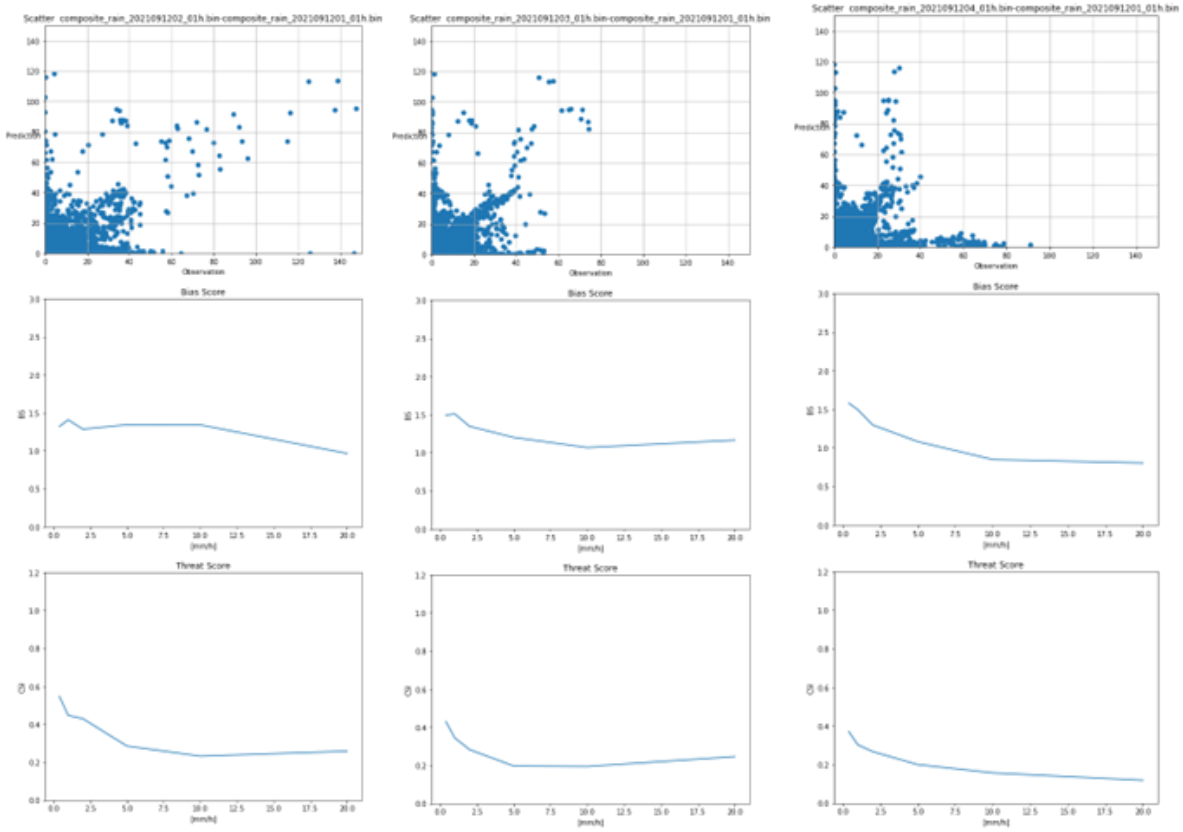


**Figure 8.** Upper) Scatter diagrams of persistency between the rainfall intensities at 02 to 04 UTC (horizontal axis) and 01 UTC (vertical axis) in the rectangles in Figure 6. Middle) Bias scores. Lower) Threat scores.

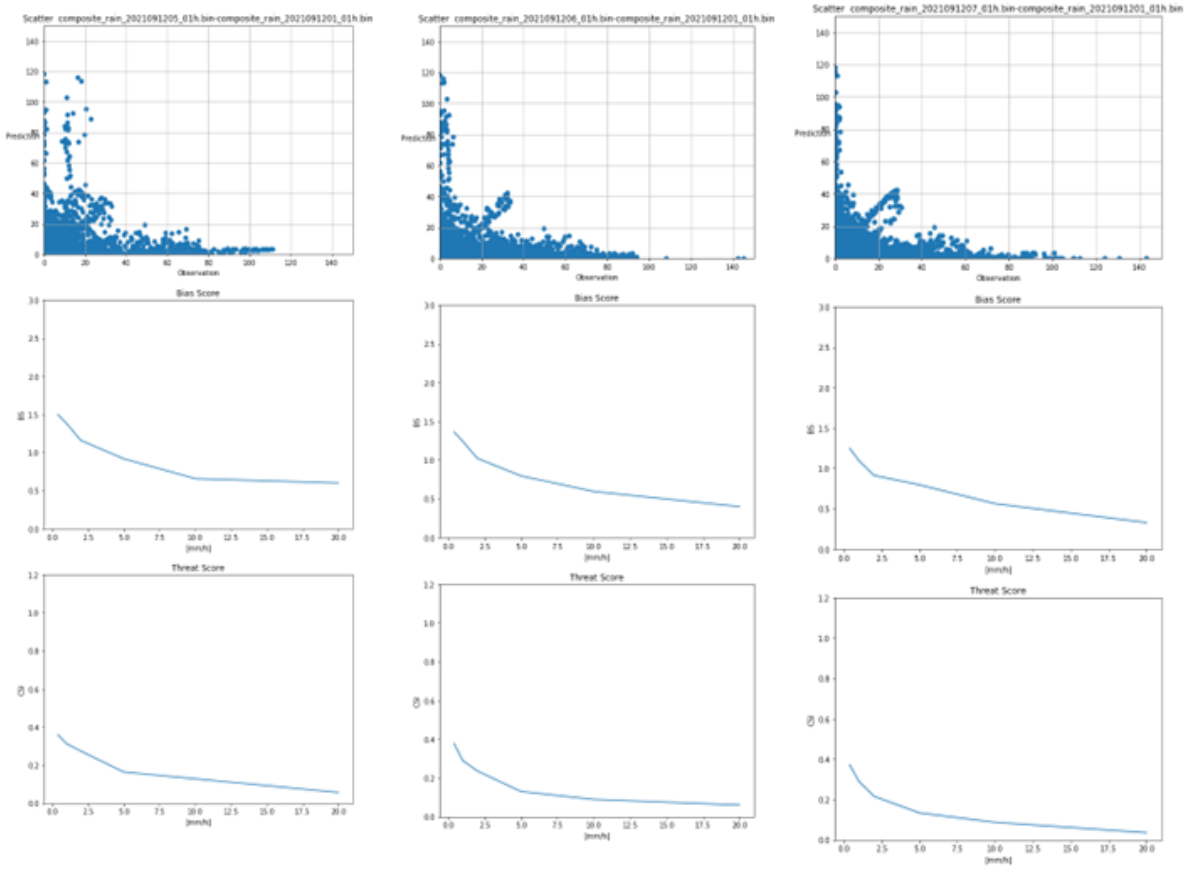


**Figure 9.** Same as in Figure 7 but for 05 to 07 UTC.

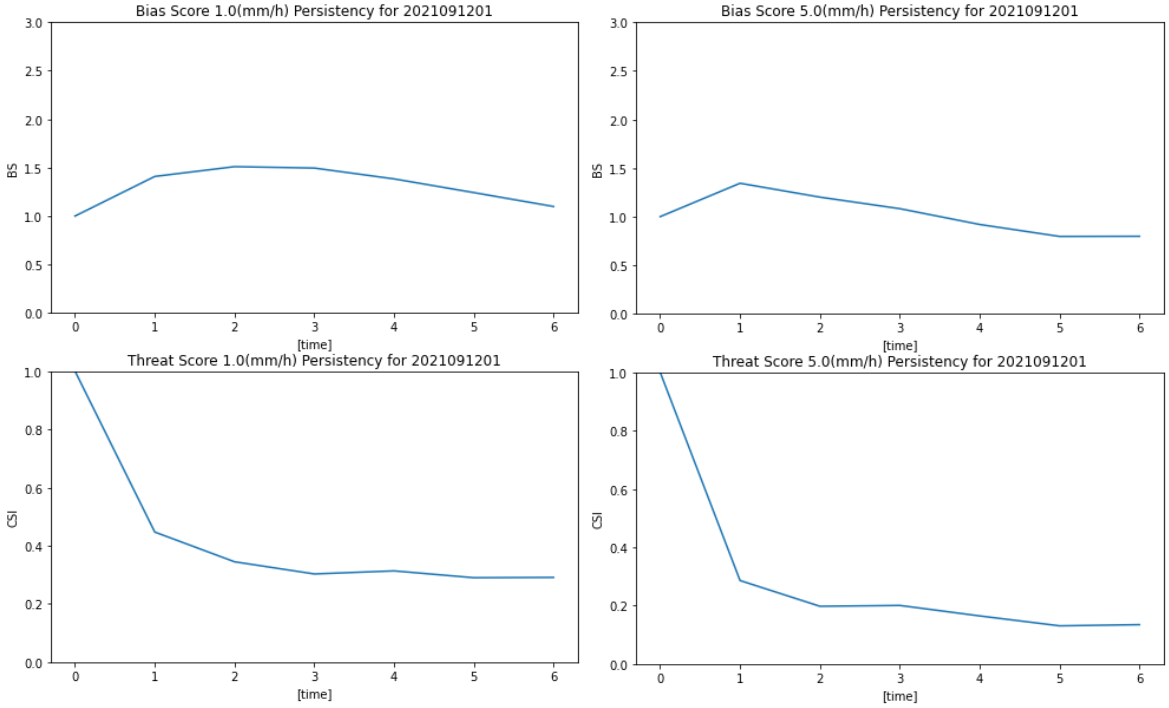


**Figure 10.** Time evolution of bias scores (upper) and threat scores (lower) of persistency for FT = 0 to 6 for 1 mm/h (left) and 5 mm/h (right) rainfall intensity threshold against 01 UTC, 2021 Sep 12.

## 4. Kinematic extrapolation by lag correlation

### *4.1. Computation of lag correlation*

For kinematic extrapolation of rainfall analyses, we followed the cross correlation method for cell tracking [14], where initial array of radar reflectivity is correlated with later array. By location the second array with the bet correlation, a motion vector for the initial array is determined. This method is widely used to calculate cloud motion vectors from satellite images ass well [15–16]. In this study, cross (lag) correlations of precipitation between two rainfall maps (e.g., 00 and 01UTC) were computed to obtain a moving vector of the precipitation areas. For the analysis domain of 15×14 degrees (330×308 grids), we computed the lag correlations at 11×10 points of every 25 grids using a computation template of 50×50 grids.

Figure 11 shows the composite rainfall analyses at 00 and 01 UTC on September 12, 2021 (corresponding to Figures 6d and 6h). An example of the computational template is shown by the yellow square over the south of Vietnam in these figures.

Figures 12a and 12b show enlarged views of the templates indicated by the squares in the lower-left corner of the figures. Positional lag correlations of rainfall intensities in these templates were calculated by shifting the template in four directions (east, west, south, and north) up to 5 grids each:

$$r_{xy} = \frac{\sum_{i=1}^{n}(x_i - \bar{x})(y_i - \bar{y})}{\sqrt{\sum_{i=1}^{n}(x_i - \bar{x})^2}\sqrt{\sum_{i=1}^{n}(y_i - \bar{y})^2}} \quad (2)$$

where $x_i$ and $y_i$ represent (the square root of) rainfall intensity at the same grid of two templates and $r_{xy}$ the correlation.

To avoid correlation coefficients being too sensitive to a few extremely intense rain grids, we applied the square root function to the rainfall intensity R before calculating the correlation coefficients. Applying the square root function in rainfall intensity in the calculation (2) is corresponding to the use of the absolute deviation in the least square

method, and this approach is known as the Huber norm in data assimilation to make the system less sensitive to outliers [17]. We also tested several functions such as the logarithm function (log(1+R)), but the results (indexes that maximize the correlation coefficients) were not so different.

Figure 12c shows the distribution of the magnitude of lag correlation coefficients when this template is shifted up to 5 grids from the center to the east, west, south, and north directions. In this figure, the correlation coefficient reaches a maximum value of 0.75 when the precipitation areas at 00 UTC are shifted to four grids to the west (x = –4) and two grids to the south (y = –2). In other words, the moving vector of the precipitation area obtained from these two figures is approximately 4.5 (2√5) grids to the west-southwest.

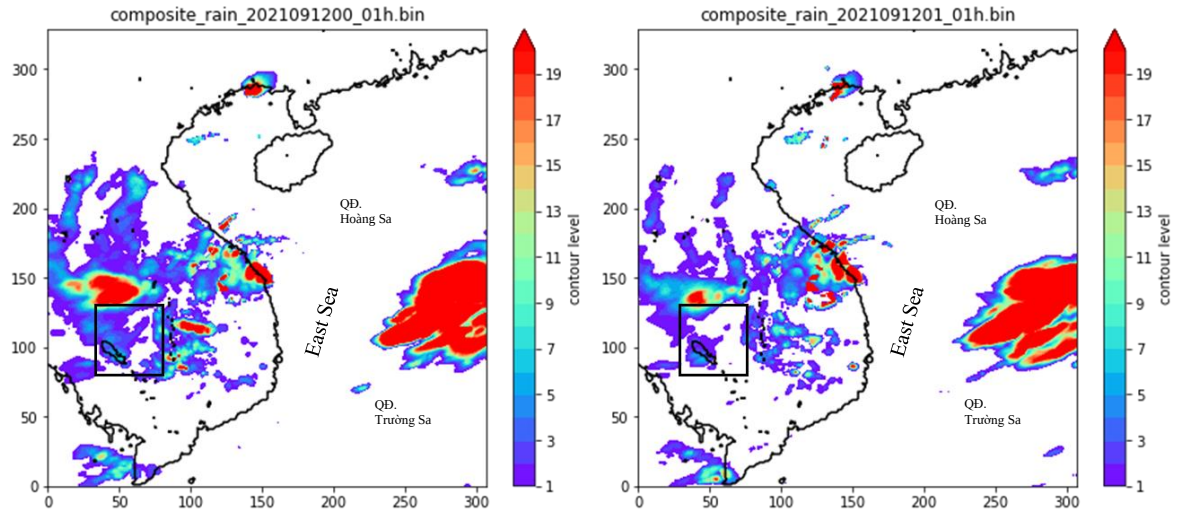


**Figure 11.** Composite rain at 00 UTC and 01 UTC, 2021 Sep 12. Black squares indicate the template to compute the lag correlation. Black lines indicate the contour of 0.5 of the land use in the WRF3kmIFS–DA model.

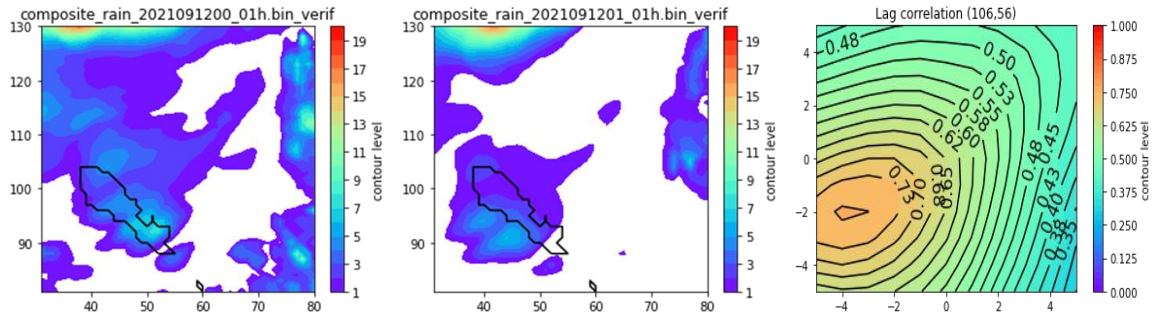


**Figure 12.** Enlarged view of composite rain in the template at 00 UTC and 01 UTC, 2021 Sep 12, and lag correlation coefficients at a grid point of (106, 56).

The computation points were changed by 25 grids to find the amount of movement with similar maximum correlation coefficients at 11×10 points in the region. The Cressman interpolation to the original grids is used:

$$z_p = \frac{\sum_{i=1}^{n} w_i z_i}{\sum_{i=1}^{n} w_i} \tag{3}$$

where $w_i$ is the weight expressed by the following function of the square of the distance between the interpolated points and rainfall grids:

$$w_i = 1 + (x_i - x_p)^2 + (y_i - y_p)^2 \quad (4)$$

Here, the weights of the calculation points at which the maximum correlation coefficient value was less than 0.3 or the number of rainfall grids in the template was less than 10% were set to zero (shown by white masks in Figure 13). Figure 14 indicates the distribution of the indexes interpolated to the original analysis grids of 330×308.

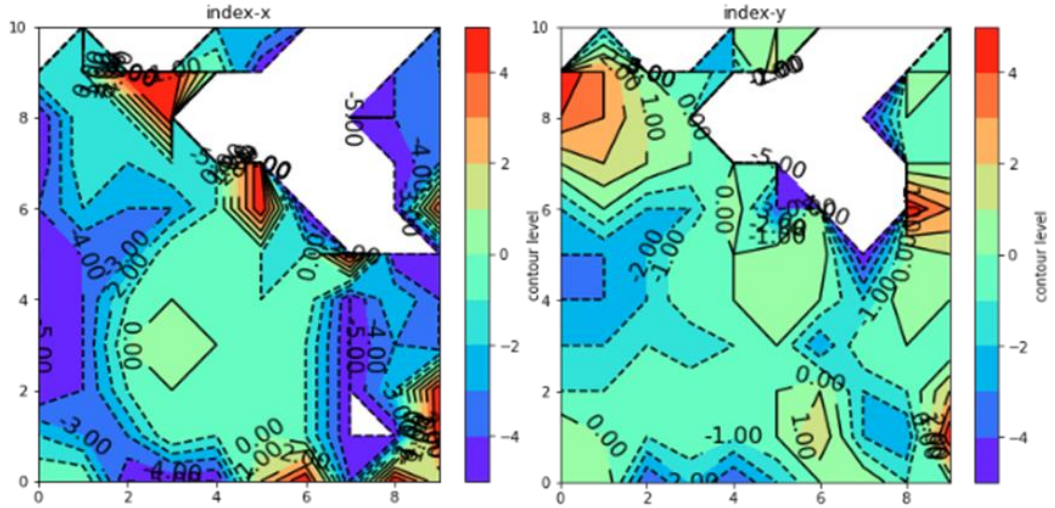


**Figure 13.** Distribution of lag-indexes which maximize the correlation coefficients at 11×10 points with intervals of 25 grids. White masks indicate the points at which the maximum correlation coefficient value was less than 0.3 or the number of rainfall grids in the template was less than 10 %.

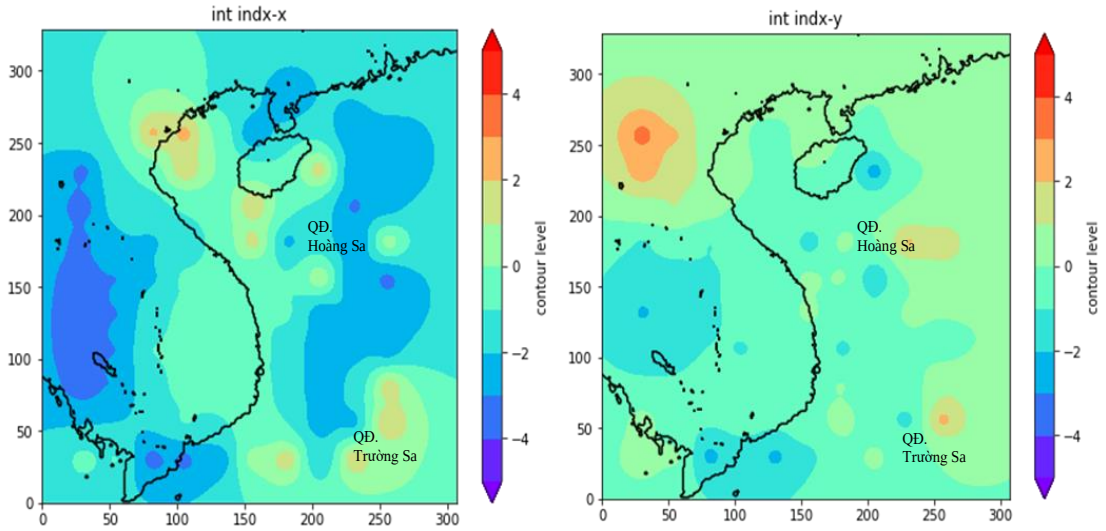


**Figure 14.** Interpolated lag indexes between 00 and 01 UTC rain map.

## *4.2. Consistency check with NWP winds*

The lag indexes that maximize the correlation coefficients may have erroneous patterns due to local extremum. To discard such unrealistic movement of rainfall area, we applied quality control using the NWP model to forecast winds. Moving vectors in the opposite directions to the NCHMF regional NWP (WRF3kmIFS-DA) winds at 700-hPa level were considered to be zero. Figure 15 indicates 700 hPa wind at 01 UTC September 12 predicted by WRF3kmIFS-DA, whose initial time is 12 UTC September 11 (FT = 13). Corresponding

to the weak tropical cyclone in the central part of Vietnam, both zonal winds (U700; left panel) and meridional winds (V700; left panel) show dipole patterns which suggest counterclockwise rotation. Figure 16 shows the resultant quality-controlled lag indexes corresponding to the moving vector components of rainfall areas. Some westward movements in the south of the tropical cyclone and northward movements in the northwest of the tropical cyclone are removed.

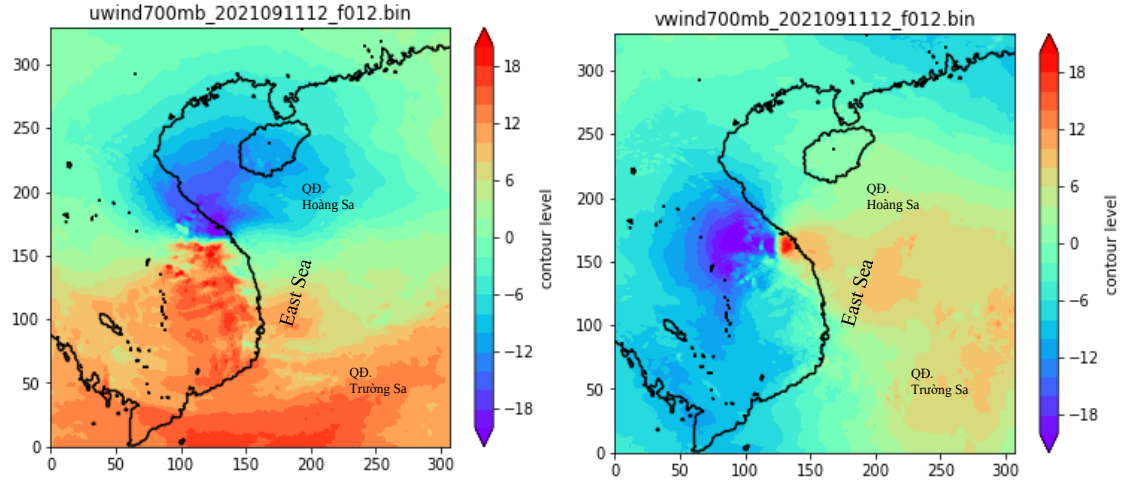


**Figure 15.** WRF3kmIFS-DA 700 hPa winds at 01 UTC: (a) U700, (b) V700.

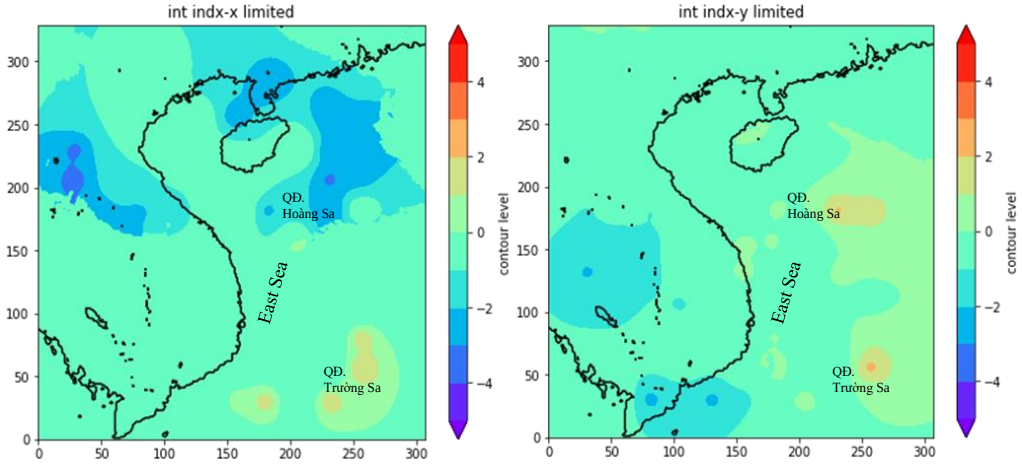


**Figure 16.** Same as Figure 13, but quality-controlled by consistency with the sign of (U700, V700).

### *4.3. Kinematic extrapolation*

The aforementioned moving vector components are used to kinematically extrapolate the rainfall areas at 01 UTC. For extrapolation, we determine an upstream point for each grid by multiplying the moving vector components by extrapolation time (i.e., linear extrapolation), and then replace the rainfall amount at the grid with the value at the corresponding upstream point.

Figure 17 shows a map of precipitation for 02-07 UTC (FT = 1-6) on 12 September 2021, obtained by the kinematic extrapolation. Corresponding to the counterclockwise rotation around the tropical cyclone, rainfall areas in the eastern part of the figure extend northward or westward slightly while most of rainfall areas over Vietnam remain or slowly move southward.

We conducted a verification of the kinematic extrapolation similar to the persistency. Figures 18 and 19 show scatter diagrams, bias scores, and threat scores for extrapolation

against rainfall analysis from 02 UTC (FT = 1) to 07 UTC (FT = 6). Seemingly these figures are not so different from the corresponding figures for persistency (Figures 7 and 8), but small differences are seen in the scatter diagrams and scores. Since kinematic extrapolation does not change the frequency of rainfall intensity, no significant differences are seen in the bias scores. On the other hand, threat scores of extrapolation for 1 mm/h and 2 mm/h at FT = 1 were slightly better than persistency. Figure 20 shows the time evolution of bias scores (upper) and threat scores (lower) of extrapolation for 1 mm/h and 5 mm/h rainfall intensity against the rainfall analysis at the same time. Threat scores of extrapolations for 1 mm/h at FT = 1 were slightly better than persistency, but no improvements are obtained in other time ranges in this case.

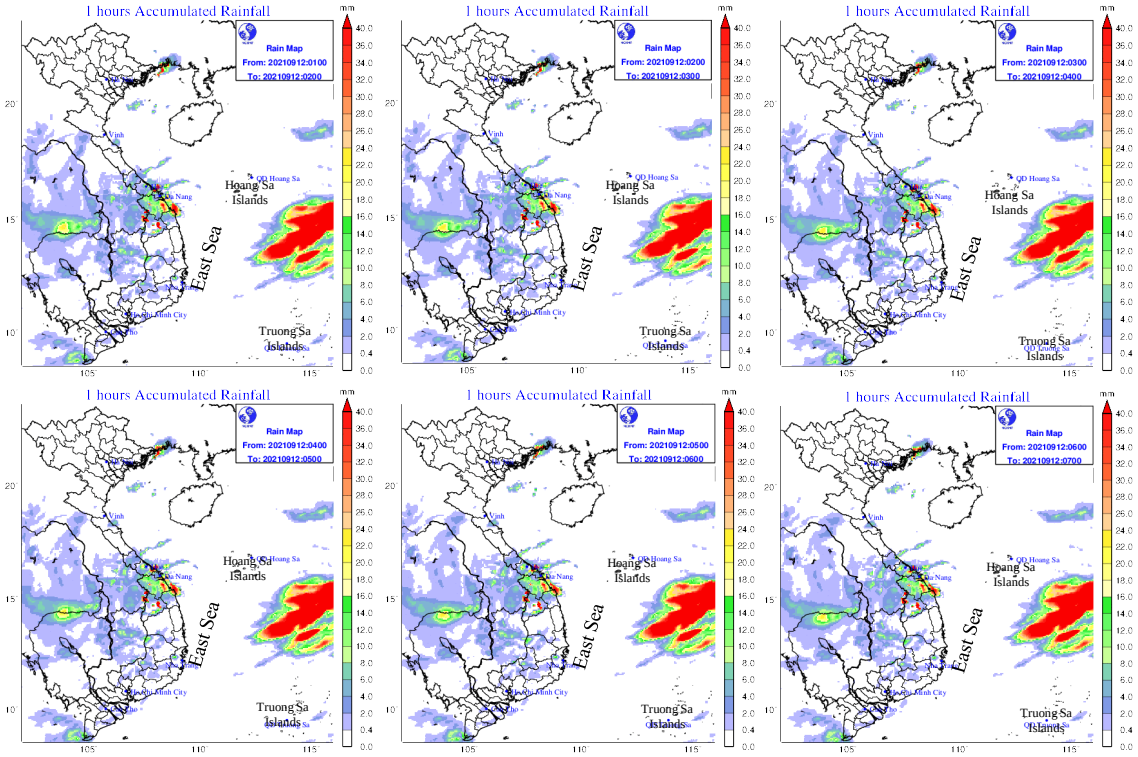


**Figure 17.** Composite rains by kinematic extrapolation for 02 to 07 UTC, 2021 September 12.

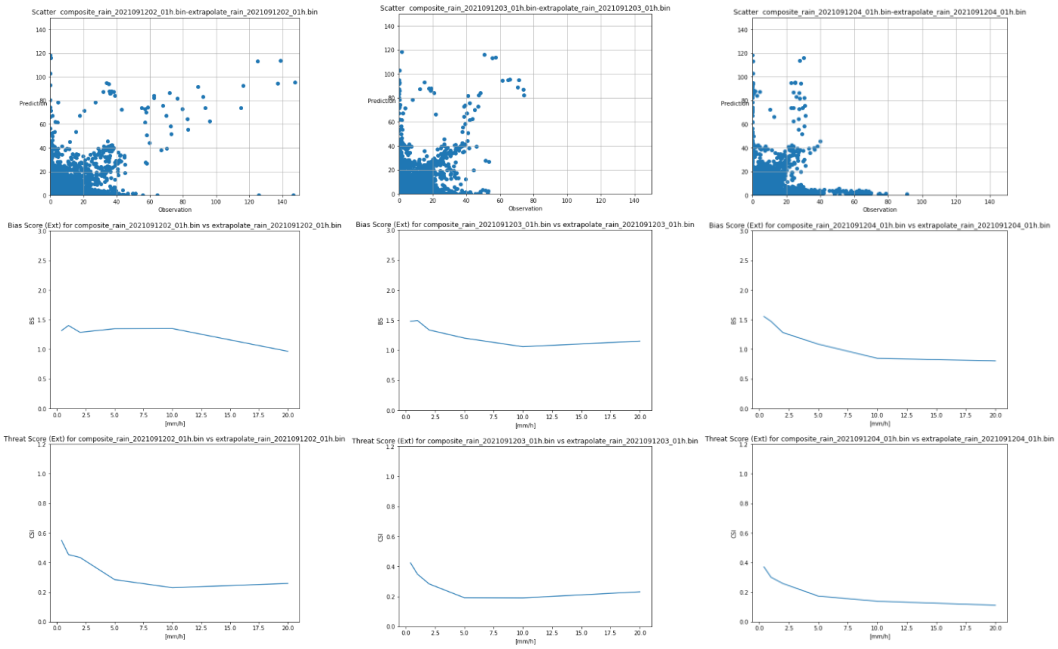

**Figure 18.** Same as Figure 8 but for extrapolation for 02 to 04 UTC (FT = 1 to 3).

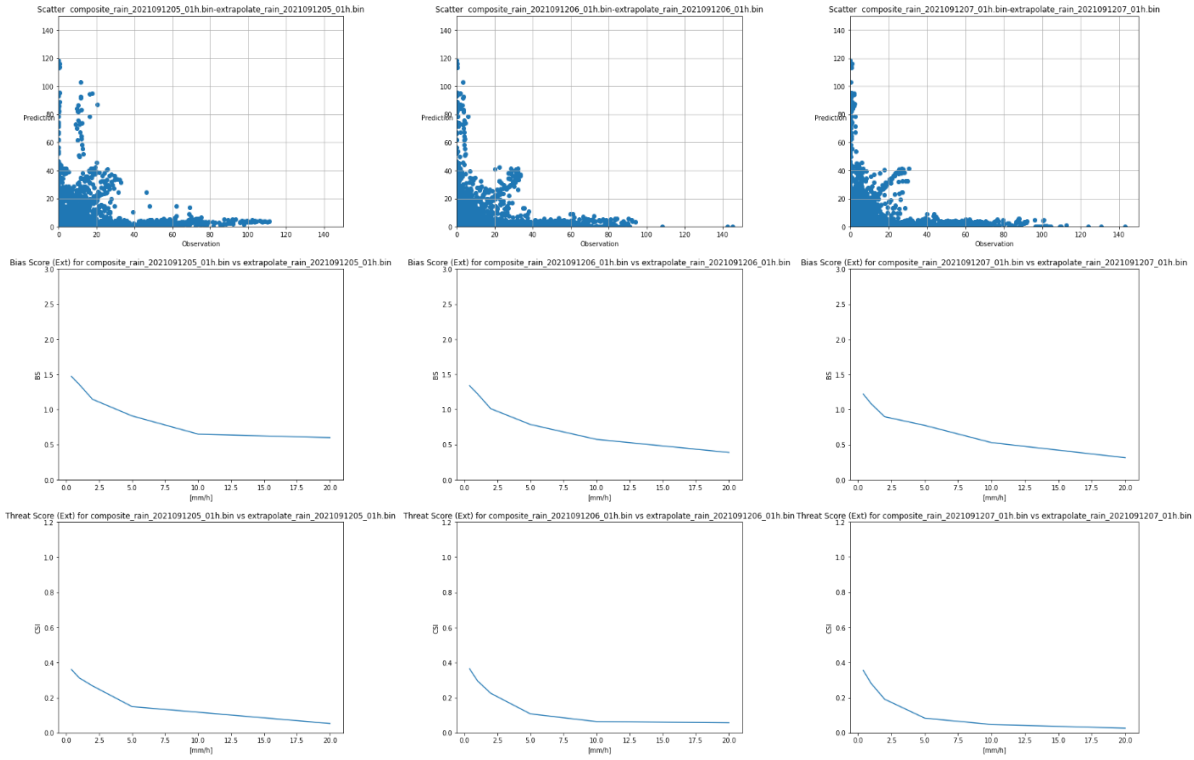


**Figure 19.** Same as Figure 18 but for 05 to 07 UTC (FT = 4 to 6).

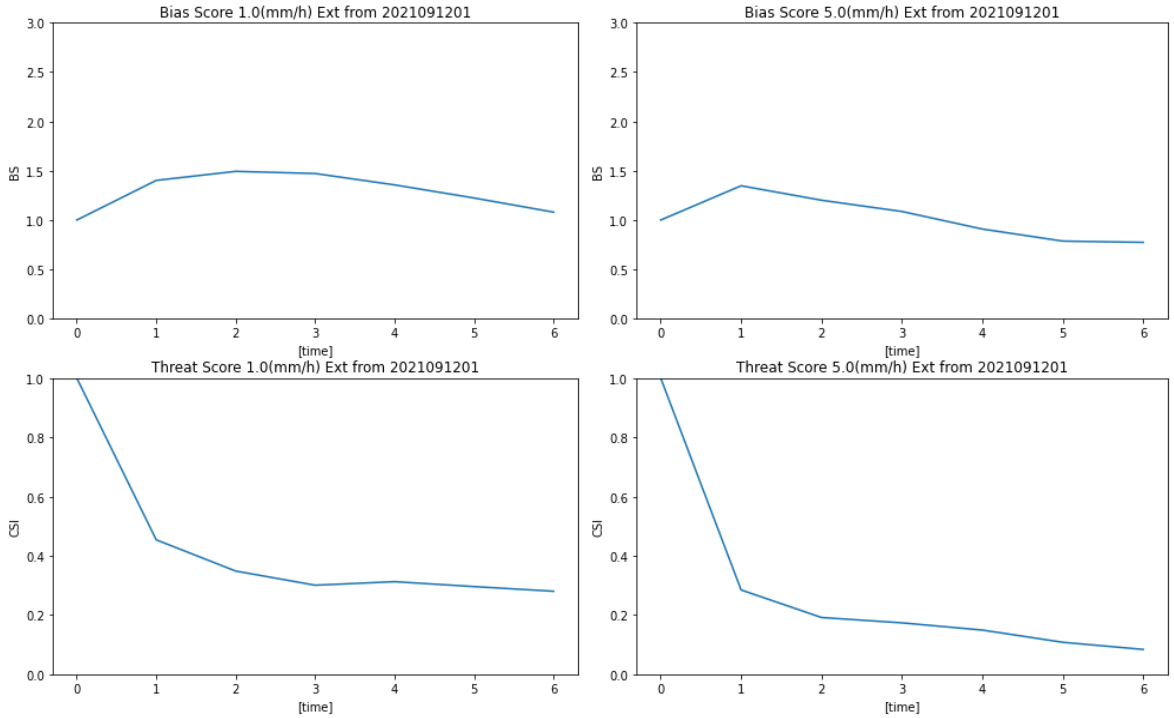


**Figure 20.** Same as Figure 10 but for extrapolated rains.

## 5. Merge with NWP

### *5.1. Regional NWP at NCHMF*

At NCHMF of VNMHA, 72-hour forecasts by a regional NWP model (WRF-ARW) with a horizontal resolution of 3 km are conducted operationally four times a day. The initial condition is prepared by 3D-VAR at 00, 06, 12, and 18 UTC, assimilating observations (SYNOP) in Vietnam and NCEP observation data (PREPBUFR), whose first guess is given

by a 6-hour assimilation cycle (WRF3kmIFS-DA). The lateral boundary condition is given by the ECMWF's global forecast model (IFS). Due to the data latency of IFS forecasts, the WRF 3 km uses IFS forecasts from the previous 12UTC for 00 and 06 UTC forecasts, and IFS forecasts from the previous 00 UTC for 12 and 18 UTC forecasts. For the 00 UTC initial forecast, the data assimilation starts at 04 UTC, the forecast starts at 05 UTC, and computation and post-processing end at around 0630 UTC.

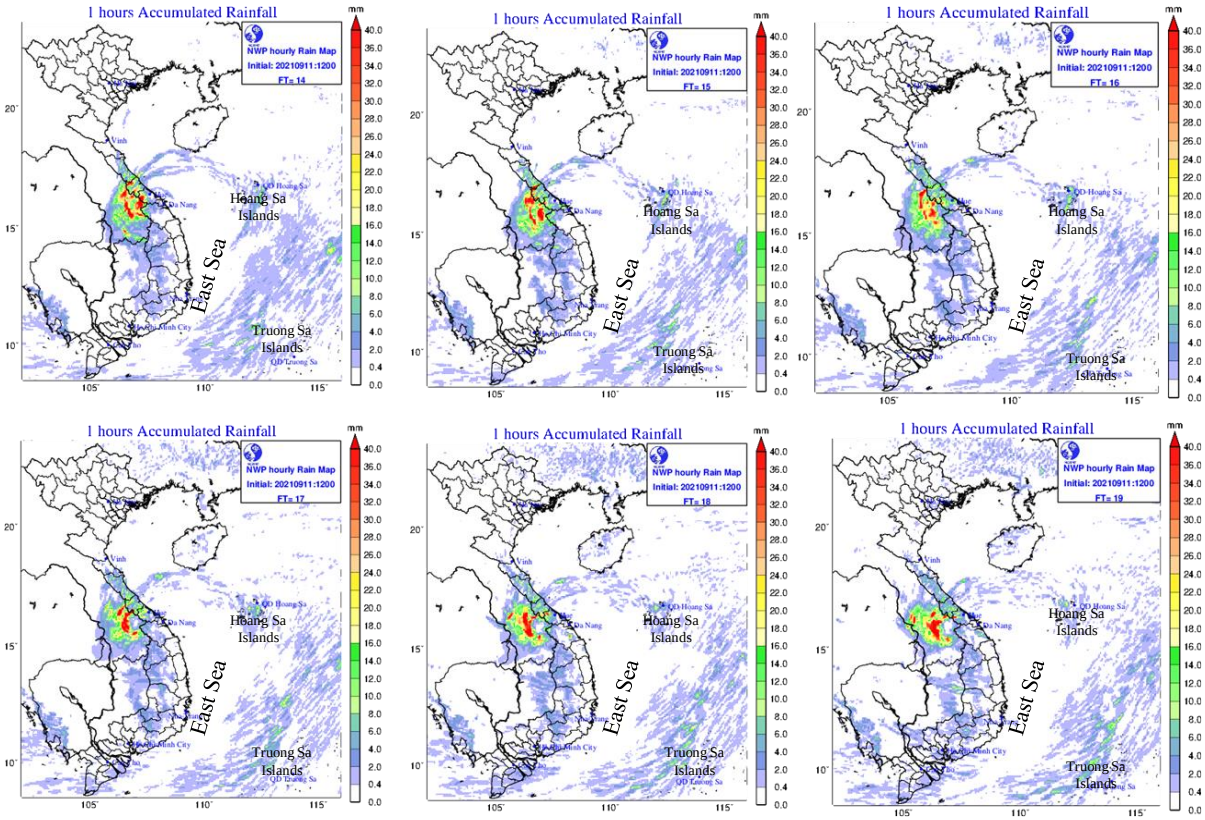


**Figure 21.** Hourly precipitation forecast by WRF3kmIFS-DA for 02 to 07 UTC, 2021 September 12.

Considering the timing to obtain the forecast of WRF3kmIFS-DA, we assume that for 00 UTC's VSRFP, we use WRF3kmIFS-DA whose initial time is 12 UTC of the day before. For the development of the VSRFP system, we re-ran WRF3kmIFS-DA from 12 UTC, 2021 September 11 with hourly outputs of the precipitation data. Figure 21 shows the hourly precipitation forecast by WRF3kmIFS-DA for 02 to 07 UTC (FT = 14 to 19), 2021 September 12. Comparing the corresponding rainfall analysis (Figure 6), intense rains overestimated by satellite are not seen over the sea in NWP-predicted rains. Scatter plot and verification scores for 01 UTC to 07 UTC (FT = 13 to 19 from 12 UTC the day before) against the rainfall analysis are shown in Figures 22 and in 23. The correlation between the analysis and NWP is not as good as extrapolation for early time ranges. The bias scores of NWP are around 1.0 for weak rains, but it decreases for intense rains after 05 UTC. Since this verification does not allow any positional lags in the computation of the scores, threat scores for intense rains are very small.

Figure 24 shows the time evolution of bias scores (upper) and threat scores (lower) of NWP for 1 mm/h and 5 mm/h rainfall intensity. Both bias and threat scores of NWP are relatively flat. For 1 mm/h, bias scores are around 1.0 and threat scores are around 0.2. For 5 mm/h, bias scores are in the range of 0.5 to 1.0 but threat scores are around 0.1 after FT = 3.

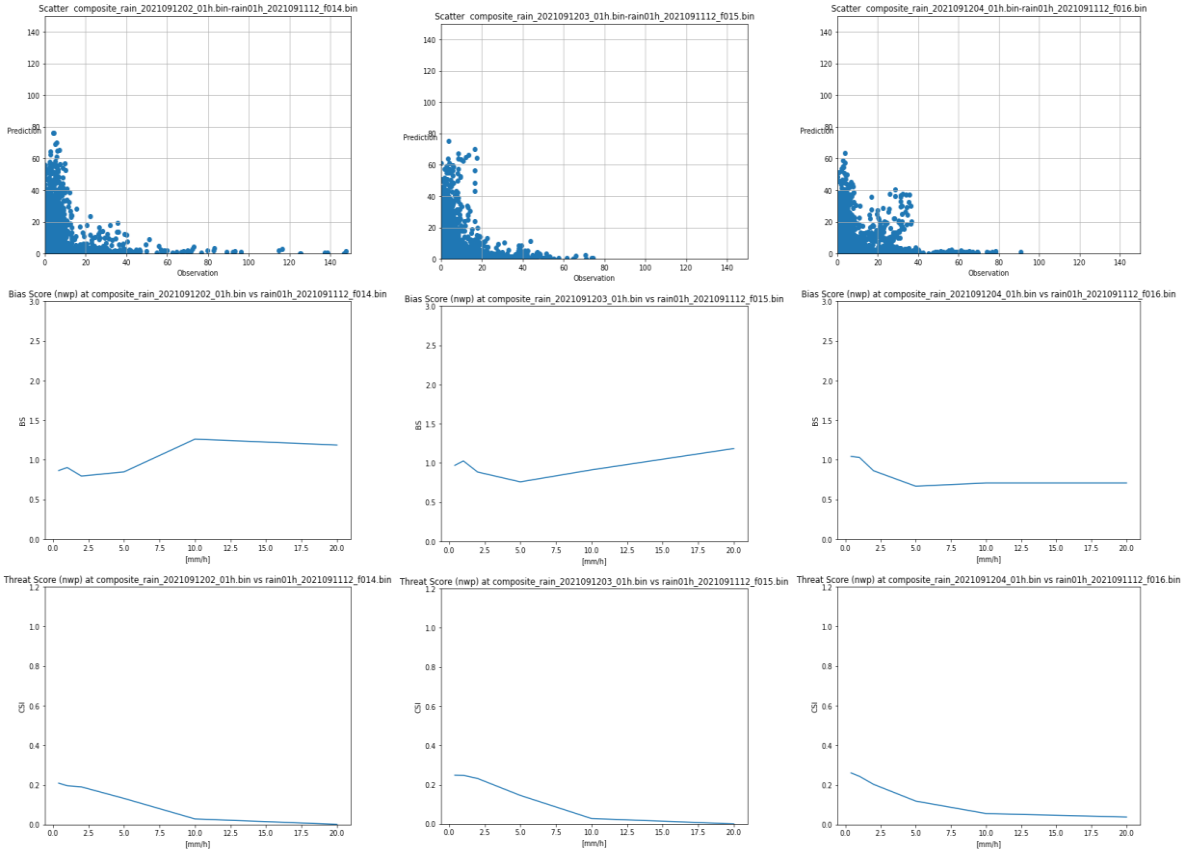


**Figure 22.** Same as Figure18 but for NWP rains for 02 to 04 UTC (FT = 14 to 16 from 12 UTC of the day before).

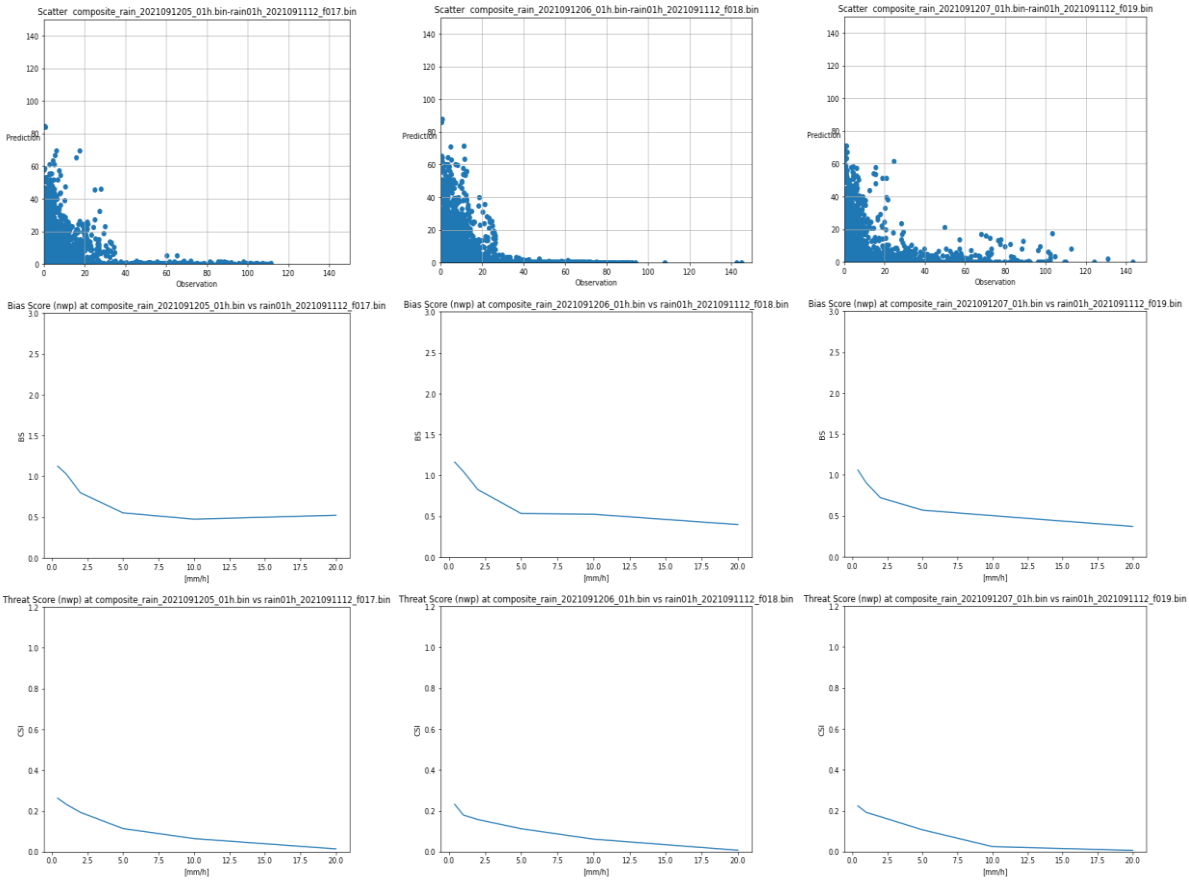


**Figure 23.** Same as Figure 22 but for 05 to 07 UTC (FT=17 to 19 from 12 UTC of the day before).

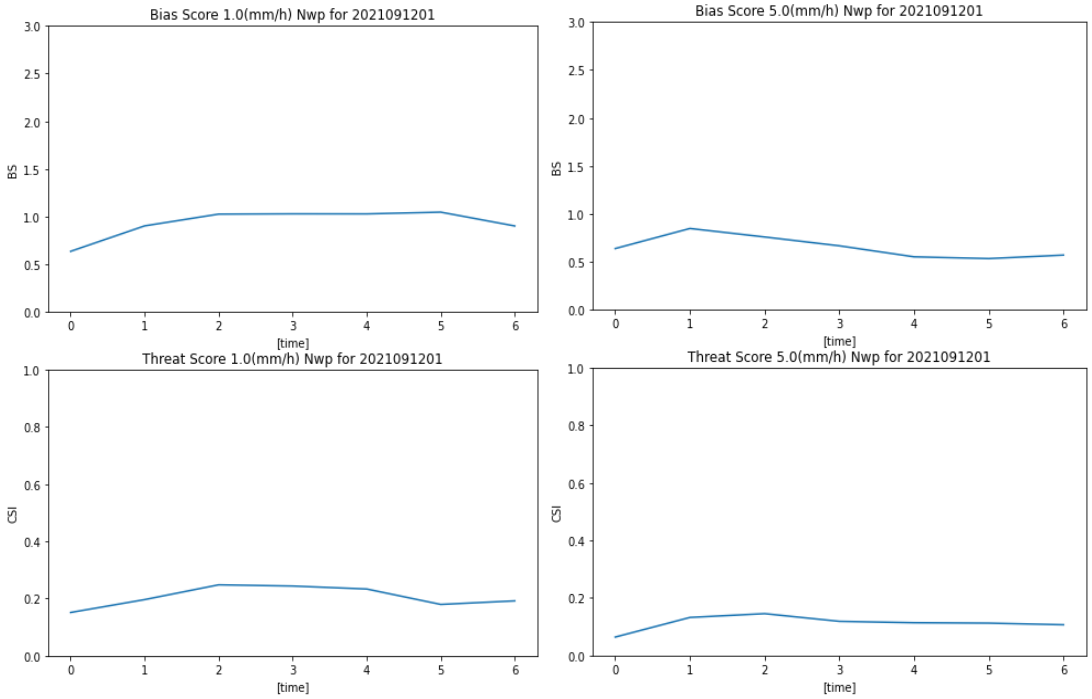


**Figure 24.** Same as Figure 20 but for NWP rains by WRF3kmIFS-DA.

### *5.2. Merge of extrapolated rains and NWP*

As the development of a very short-range forecast of precipitation system (Figure 1), we merged kinematically extrapolated precipitation rainfall with NWP model-predicted rainfall by the WRF3kmIFS-DA. The merged intensity (Mrg) is given by a weighted mean of kinematic extrapolation (Exp) and numerical weather prediction (Nwp):

$$\mathrm{Mrg} = \mathrm{Exp} \times w + \mathrm{Nwp} \times (1 - w) \quad (5)$$

where $w$ is the weight parameter. In JMA's VSRFP, the magnitude of $w$ is dynamically determined based on the local accuracy of NWP (Figure 25).

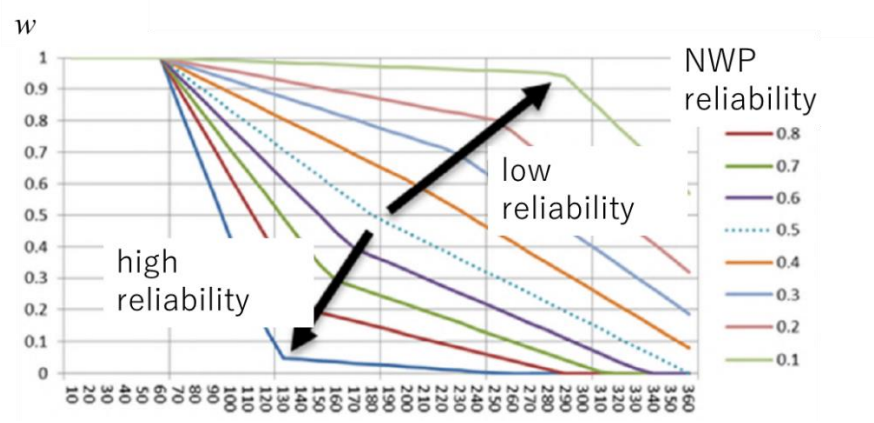


**Figure 25.** Weight parameter in JMA7s VSRFP. Reproduced from Tsujimura (2019) [8].

Here, the NWP reliability is determined by the ratio of NWP and Extrapolation scores (for detail, see [8]). In our prototype system, we reduced the weight parameter w linearly from 1.0 at FT = 2 to 0.0 at FT = 6 for simplicity, i.e., 0.75 at 04 UTC (FT = 3), 0.5 at 05 UTC (FT = 4) and 0.25 at 06 UTC (FT = 5). This procedure roughly corresponds to assuming the NWP reliability around 0.4. As shown in Figure 26, the merged rains are identical to the extrapolation until FT = 2, and then gradually approach NWP rains from FT = 3 to 5, and finally agree with NWP at FT = 6.

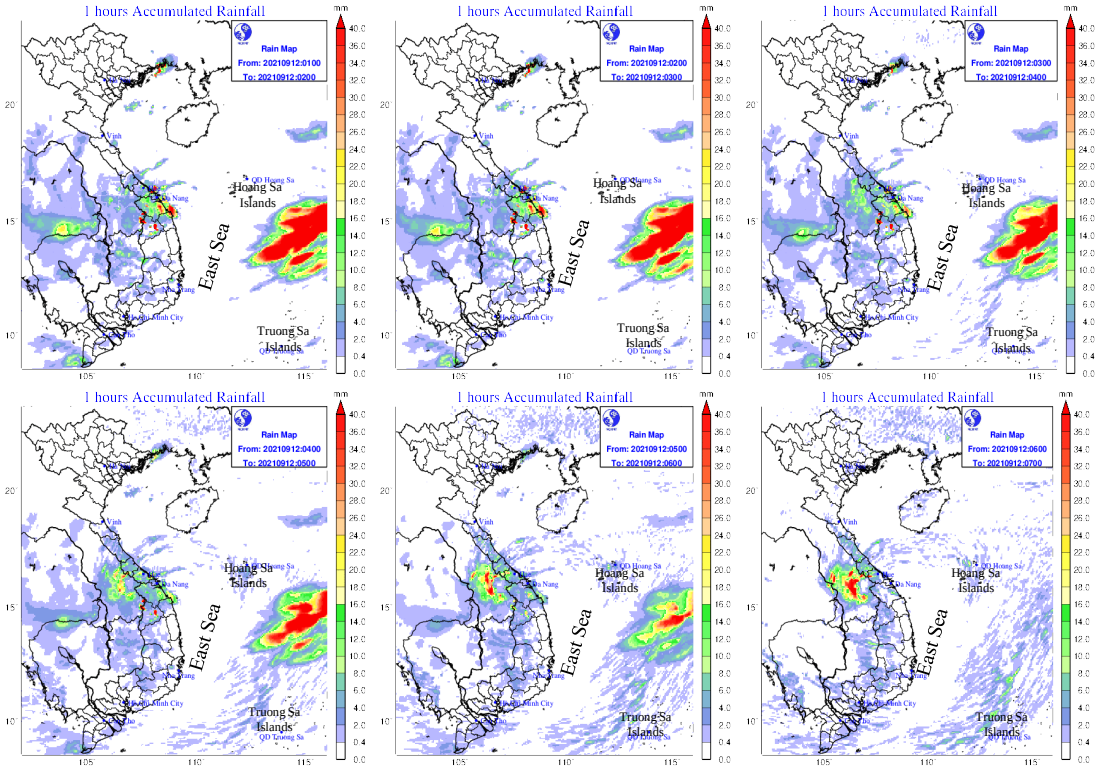


**Figure 26.** Same as Figures 15 and 18 but by very short-range forecast of precipitation.

Figure 27 shows the scatter plot and verification scores of merged rains at 04, 05 and 06 UTC (FT = 3 to 5) against the rainfall analysis. The bias scores of merged rains are slightly larger than extrapolation or NWP for weak rains but smaller for intense rains. This is due to the weighted averaging of two values, which moderates intense rains. Threat scores are better than extrapolation for weak rains. This improvement is attributable to the effect of the ensemble mean in the weighted average.

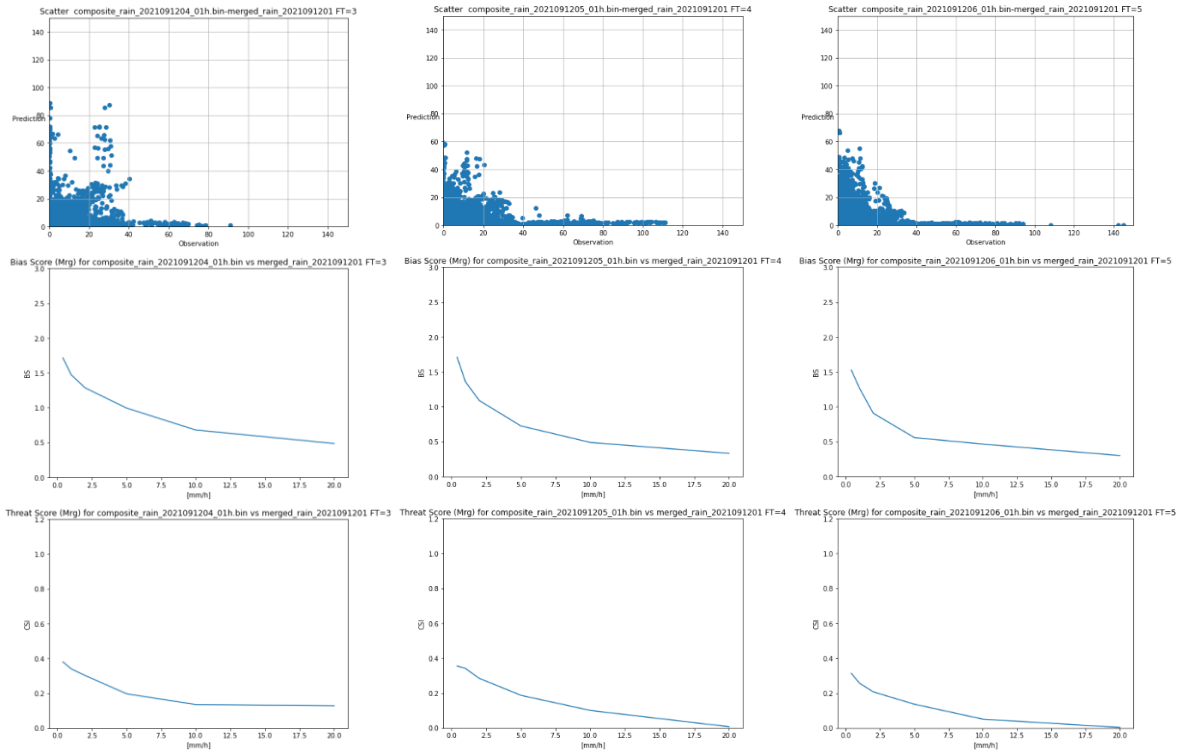


**Figure 27.** Same as Figure 17 but for VSRFP for 04 to 06 UTC (FT = 3 to 5).

Figure 28 shows the time evolution of bias scores (upper) and threat scores (lower) of merged rains for 1 mm/h and 5 mm/h intensities. Bias scores for 1 mm/h are almost the same as an extrapolation and larger than NWP. Threat scores for 1 mm/h are better than extrapolation for FT = 3 and 4, and better than NWP for all time ranges. Threat scores for 5 mm are better than both extrapolation and NWP for all time ranges.

### *5.3. Verification for the different initial time*

In the former subsections, we computed the lag correlation between the two composited hourly rainfall distributions at 00 and 01 UTC and extrapolated the rains from 02 to 07 UTC. To check the performance of this system for a different initial time, we conducted similar lag correlation procedures for two composited rain fields at 01 and 02 UTC, and extrapolated the rain fields at 02 UTC for 03 to 08 UTC. As for NWP forecast, forecast from the same NWP whose initial time of 12 UTC 11 September was used (FT = 15 to 20).

Figure 29 indicates time evolution of threat scores of extrapolations (upper) and merged rains (lower) for FT = 0 to 6 (02 to 08 UTC) for 1 mm/h (left) and 5 mm/h (right) rainfall intensity. The same tendencies as in the initial time of 01 UTC were obtained; for 1 mm/h merged rains were better than extrapolation at FT = 3 and 4, and for 5 mm/h merged rains were better than extrapolation at after FT = 3-time ranges.

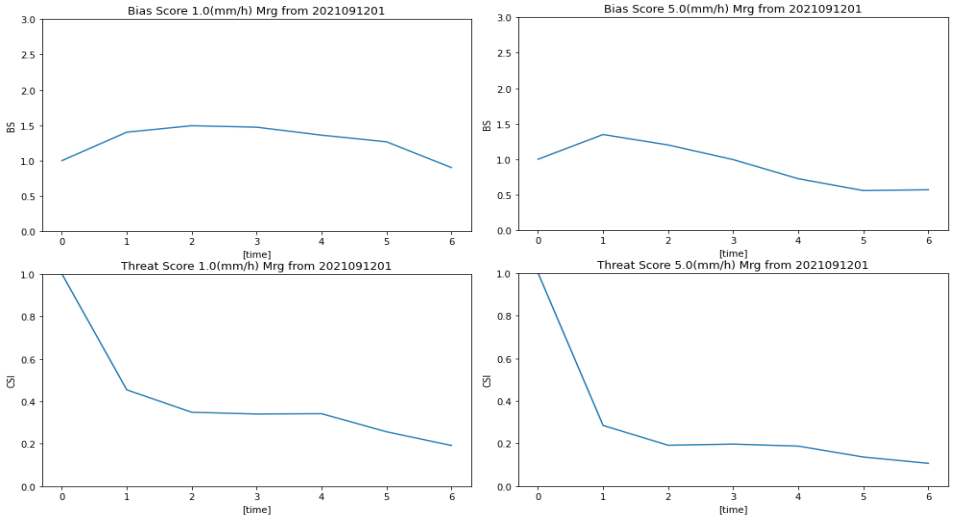


**Figure 28.** Same as Figure 20 but by VSRFP.

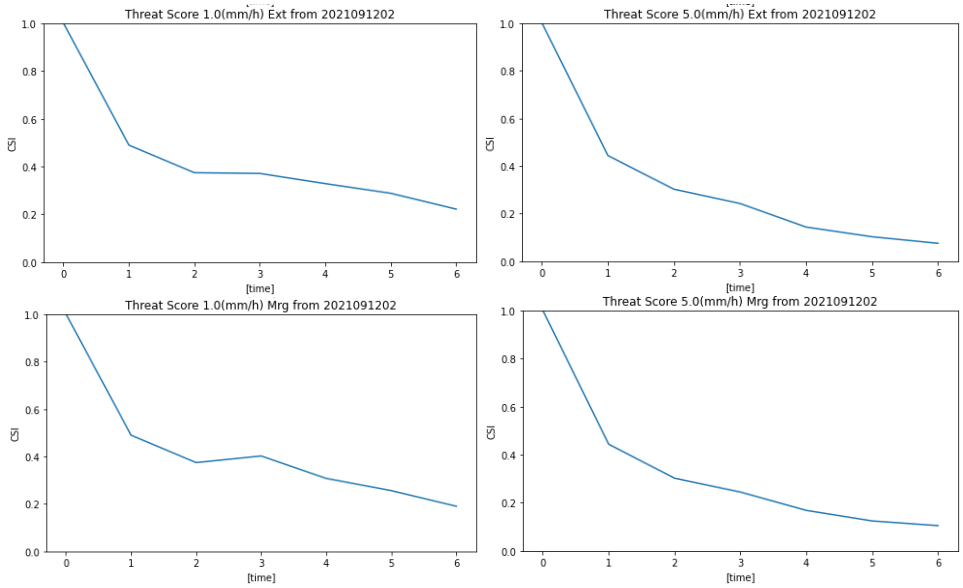


**Figure 29.** Upper) Time evolution of threat scores of extrapolations from 02 UTC to 08 UTC for FT = 0 to 6 for 1 mm/h and 5 mm/h rainfall intensity threshold against rainfall analysis. Lower) Same as in upper panels but by VSRFP.

## 6. Summary and concluding remarks

Toward the very short-range forecast of precipitation, we prepared a one-hour composite rainfall analysis using AWS, radar, and satellite data for the case of heavy rainfall event over central Vietnam on 11 to 13 July 2021. Moving vectors of rainfall area were estimated by computing lag correlation coefficients in the template between the two rainfall distributions at 00 and 01 UTC, and the indexes which maximize the lag correlation were interpolated to the original grid of 5 km. Quality control of the moving vectors was made by checking the consistency between the moving directions and NWP winds at 700 hPa level. Extrapolated rains were merged with rainfall forecast by VNMHA's operational NWP (WRF3kmIFS-DA), with a weight function which increases the weight of NWP linearly from FT = 2 to FT = 6. Merged rainfall outperformed extrapolation at least weak to moderate rains such as 1 and 5 mm/h.

In this paper, we selected a heavy rainfall case in July 2021 brought by a weak tropical cyclone which slowly approached central Vietnam. Different from mid-latitude synoptic disturbances which move eastward by the prevailing westerly, the major rainfall areas did not move eastward and stalled over the central Vietnam, though individual clouds around the tropical cyclone rotate counterclockwise. Generally, if the major rainfall area is advected by synoptic winds, the performance of the persistency is soon deteriorated, however in this case, the persistency kept its performance, and the extrapolation did not clearly outperform the persistency. More cases need to be studied to show the advantage of extrapolation based on the lag correlation method. In this first trial, we applied a simple linear method for extrapolation to detect the upstream point. Recently, [18] proposed a new method for cell tracking, where the cross-correlation method is used to obtain average moving vectors and the optimal over lapping area method is applied to modify the vector for each cell motion. A more sophisticated method may improve the performance of kinematic extrapolation. In the merger process, we used a simple linear function for weight parameters. As in the JMA's VSRFP system [8], there is room for much improvement in this approach as well.

As shown in threat scores, the precipitation forecast by WRF3kmIFS-DA was not necessarily good in this case. If the performance of NWP improved, the merit of a merger should become larger. As additional tests, by considering the data latency at the timing of 01 UTC (and 02 UTC), we used the NWP forecast whose initial time is 12 UTC of the day before (11 July 2021) for the merger process. This means that NWP forecasts with FT = 16 to 19 (17 to 20) were used. Supposing an operational time schedule, where the computation and post processing ends at around 6.5 hours later from the initial time, we can use the 18 UTC initial forecast after 02 UTC. In the near future, we will test the use of the latest NWP forecasts in the daily operational test.

**Author Contributions**: Author Contributions: Conceptualization, K.S.; methodology, K.S.; validation, K.S., M.K.H.; AWS data curation, M.K.H., K.S.; Radar data curation, M.K.H., K.S.; Satellite data curation, M.K.H., K.S.; NWP data curation, M.K.H., K.S.; writing–original draft preparation, K.S.; writing–review and editing, D.D.T., M.K.H.; supervision, D.D.T.; project administration, K.S., D.D.T.; All authors have read and agreed to the published version of the manuscript.

**Funding:** This research was performed under the Japan International Cooperation Agency (JICA) Project for "Strengthening Capacity in Weather Forecasting and Flood Early Warning System in the Social Republic of Vietnam". Kazuo Saito was partly supported by Grant-in-Aid for Scientific Research (C) (21K03657K; Study on the mechanisms of the pre-typhoon precipitation enhancement) from the Japan Society for the Promotion of Science (JSPS). Mai Khanh Hung and Du Duc Tien were sponsored by the Ministry of Natural Resources and Environment (intervention code TNMT.2022.06.02, title of the project "Research and innovate technology to the quantitative forecast of precipitation due to typhoon, tropical

depressions by high-resolution numerical model combining data assimilation of radar, satellite, surface and upper-air observations").

**Acknowledgments:** The authors thank Nguyen Vinh Thu and Mai Van Khiem of the Viet Nam Meteorological and Hydrological Administration, Kenji Akaeda, leader of JICA team, and Michihiko Tonouchi, Kiichi Sasaki of the Japan Meteorological Business Support Center (JMBSC) for their support on the JICA project. Thanks are extended to Yasutaka Makihara of JMBSC for their comments on the kinematic extrapolation of rainfall areas. Comments by two anonymous reviewers improved the quality of this paper.

**Conflicts of Interest:** The authors declare no conflict of interest.

**References**

1. Tonouchi, M.; Kasuya, Y.; Tanaka, Y.; Akatsu, K.; Akaeda, K.; Nguyen, V.T. Activities of JICA on disaster prevention and achievement of JICA project in Period 1. *VN J. Hydrometeorol.* **2020**, *5*, 1–12. Doi:10.36335/VNJHM.2020(5).1-12.
2. Mikami, M.; Ichijo, H.; Matsubara, M.; Nguyen, H.A.; Duc, L.X. A proposal of AWS maintenance and periodic calibration tools and installation of ARGs for Radar QPE calibration. *VN J. Hydrometeorol.* **2020**, *5*, 13–35. Doi: 10.36335/VNJHM.2020(5).1-35.
3. Kimpara, C.; Tonouchi, M; Hoa, B.T.K.; Hung, N.V.; Cuong, N.M.; Akaeda, K. Quantitative precipitation estimation by combining rain gauge and meteorological radar network in Vietnam. *VN J. Hydrometeorol.* **2020**, *5*, 36–50. Doi:10.36335/VNJHM.2020(5).36-50.
4. Saito, K.; Hung M.K.; Hung N.V.; Vinh N.Q.; Tien D.D. Heavy rainfall in central Viet Nam in December 2018 and modification of precipitation analysis at VNMHA. *VN J. Hydrometeorol.* **2020**, *5*, 65–79. Doi:10.36335/VNJHM.2020(5).65-79.
5. Hung, M.K.; Saito, K.; Khiem, M.V.; Tien, D.D.; Hung, N.V. Verification of GSMaP data in precipitation nowcasting at Vietnamese National Center for Hydro-Meteorological Forecasting. *VN J. Hydrometeorol.* **2020**, *5*, 80–94. Doi: 10.36335/VNJHM.2020(5).80-94.
6. Kigawa, S. Analysis and forecasting techniques of high-resolution precipitation nowcasting. *Sokko-jiho* **2014**, *81*, 55–76. Available online: https://www.jma.go.jp/jma/kishou/books/sokkou/81/vol81p055.pdf. (In Japanese)
7. Saito, K.; Makihara, Y. On the very short range forecast of precipitation at JMA. *J. Water Env. Japan* **2007**, *30(5)*, 230–235. Available online: https://www.jswe.or.jp/publications/journals/contents/2007/index.html) (In Japanese)
8. Tsujimura, Y. Modification of very short range forecast of precipitation. *Forecasting Technology Training Textbook, JMA* **2019**, *24*, 146–153. Available online at https://www.jma.go.jp/jma/kishou/books/yohkens/24/chapter7.pdf. (In Japanese)
9. Li, P.W.; Wong, W.K.; Cheung, P.; Yeung, H.Y. An overview of nowcasting development, applications, and services in the Hong Kong Observatory. *J. Meteor. Res.* **2014**, *28*, 859–876. Doi:10.1007/s13351-014-4048-9.
10. Japan Meteorological Agency website. https://www.jma.go.jp/jma/kishou/know/bosai/riskmap.html.
11. World Meteorological Organization. WMO guidelines on multi-hazard impact-based forecast and warning services. WMO No.1150. 2015, pp. 34. ISBN: 978-92-63-11150-0.
12. Kobayashi, R.; Duc, L.X.; Tien, P.M. Attempt to detect maintenance-need rain gauge station by double–mass analysis. *J. Hydro-Meteorol.* **2023**, *15*, 10–20.

13. Vicente, G.; Scofield, R.A.; Mensel, W.P. The operational GOES infrared rainfall estimation technique. *Bull. Amer. Meteor. Soc.* **1998**, *79*, 1881–1898. Doi:10.1175/1520-0477(1998)079<1883:TOGIRE>2.0.CO;2.
14. Rinehart, R.E.; Garvey, E.T. Three-dimensional storm motion detection by conventional weather radar. *Nature* **1978**, *273*, 287–289.
15. Hamada, T. Cloud wind estimation system summary of GMS system. *Tech. Note Meteor. Satt. Cent.* **1979**, *II–2*, 14–42.
16. Takano, I.; Saito, K. Statistical analyses of wind field obtained from short interval VISSR observations. *Tech. Note Meteor. Satt. Cent.* **1986**, *14*, 29–37.
17. Tavolate, C.; Isaksen, L. On the use of a Huber norm for observation quality control in the ECMWF 4D-Var. *Quart. J. Roy. Meteor. Soc.* **2015**, *141*, 1514–1527. Doi:10.1002/qj.2440.
18. Shimizu, S.; Ueda, H. Algorithm for the identification and tracking of convective cells based on constant and adaptive threshold methods using a new cell-merging and - splitting scheme. *J. Meteor. Soc. Japan* **2012**, *90*, 869−889. Doi:10.2151/jmsj.2012-602.